JACS
JOURNAL OF THE AMERICAN CHEMICAL SOCIETY
Article
pubs.acs.org/JACS

Seed-Mediated Growth of Shape-Controlled Wurtzite CdSe Nanocrystals: Platelets, Cubes, and Rods

Katherine P. Rice,[†] Aaron E. Saunders, and Mark P. Stoykovich*

Department of Chemical and Biological Engineering, University of Colorado, Boulder, Colorado 80309, United States

Supporting Information

ABSTRACT: Prior investigations into the synthesis of colloidal CdSe nanocrystals with a wurtzite crystal structure (wz-CdSe) have given rise to well-developed methods for producing particles with anisotropic shapes such as rods, tetrapods, and wires; however, the synthesis of other shapes has proved challenging. Here we present a seed-mediated approach for the growth of colloidal, shape-controlled wz-CdSe nanoparticles with previously unobserved morphologies. The synthesis, which makes use of small (2−3 nm) wz-CdSe nanocrystals as nucleation sites for subsequent growth, can be tuned to selectively yield colloidal wz-CdSe nanocubes and hexagonal nanoplatelets in addition to nanorod and bullet-shaped particles. We thoroughly characterize the morphology and crystal structures of these new shapes, as well as discuss possible growth mechanisms in the context of control over surface chemistry and the nucleation stage.

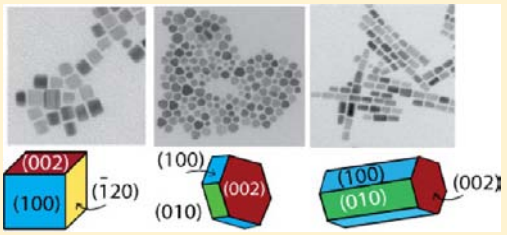

INTRODUCTION

The past few decades of research have provided clear and elegant demonstrations of the effect of composition and size on the properties of semiconductor, metal, and ceramic nanocrystals. Over the past few years, researchers have sought to extend or fine-tune these properties in a variety of ways, including by developing synthetic methods to produce multicomponent nanomaterials,[1,2] include low concentrations of dopants,[3,4] and control the nanoparticle morphology.[5−7] In metal nanocrystals, for example, the ability to create structures with sharp corners can spatially focus optical behaviors important for sensors based on the localized surface plasmon resonance (LSPR) or platforms for surface enhanced Raman spectroscopy (SERS).[8] Similarly, metal nanostructures of controlled shape can increase the exposed surface area of particular crystallographic facets, thereby dramatically enhancing the catalytic activity of the nanomaterials.[9−11] In semiconductor nanomaterials, the emission from spherical nanocrystals is isotropic, whereas nanorods and nanowires exhibit polarized luminescence,[12,13] and changes in shape can modulate overall optical and electronic properties due to changes in band structure.[14] As such materials are incorporated into new technologies, including solution-processable photovoltaics[15,16] and light-emitting devices,[17] synthetic control over the shape of the nanocrystals will be required to provide the desired optoelectronic properties and function, and will also dictate how the particles self-assemble and locally pack together thus allowing the packing density (or porosity) to be tuned within these films.[18,19]

Cadmium selenide has found favor as both a model system for study and a potentially useful material in a variety of optoelectronic applications, due in part to robust synthetic methods[20] and the ability to tune the absorption and emission behavior across the visible spectrum. CdSe also has become a useful material for studying techniques to control particle morphology during synthesis.[5−8] The material is polytypic [in general, lower-temperature syntheses favor the formation of the zincblende (zb) crystal structure, while higher reaction temperatures form the wurtzite (wz) phase], and several classes of capping ligand functional groups bind selectively to certain crystal facets, such as phosphonic acids, carboxylic acids, and amines.[21−23] These properties, when controlled in combination with techniques that regulate nanocrystal growth kinetics,[24,25] make CdSe an excellent model system for developing synthetic methods to control nanocrystal morphology and for understanding the mechanisms associated with shape-directed growth.

To date, methods of controlling the shape of CdSe have arguably met with the greatest success in particles synthesized with the cubic zincblende crystal phase, for which examples of highly faceted particles including cubes, tetrahedrons, and platelets have been demonstrated.[26−28] In contrast, efforts to synthesize different shapes for wz-CdSe have mostly been limited to nanorods[29] and nanowires,[30] structures made of elongated building blocks including tetrapods[31] and hyperbranched structures,[32] and other variations on the elongated form including teardrop- and arrow-shaped particles,[5] as well as octapodal structures.[33,34] This limited range of shapes in wz-CdSe nanocrystals most likely arises due to the underlying elongated unit cell of the hexagonal wurtzite crystal structure and the tendency to use phosphonic acid-containing surfactants that bind to specific crystal facets preferentially, both of which promote the anisotropic growth of such structures. For this

Received: March 3, 2013
Published: April 1, 2013

   dx.doi.org/10.1021/ja402240m | J. Am. Chem. Soc. 2013, 135, 6669−6676

reason, the synthesis of cubes and thin flat platelets for wz-CdSe has been challenging, requiring additional control over both the nucleation stage and the subsequent growth of the particles.

Seed-mediated techniques have been used to gain better control over the nucleation of wz-CdSe nanorods. For example, Manna and co-workers[35] have shown that nanostructures grown from CdSe and CdS seeds can produce exceptionally uniform, elongated nanorods. Furthermore the crystal structure of the seed has been shown to be important in determining the final shape; Talapin and co-workers[31] have elegantly demonstrated that the use of wz-CdSe seeds as nucleation sites for further growth of wz-CdSe can be tuned to produce nanorods, while the use of zb-CdSe seeds produces tetrapods with arms of wz-CdSe. In addition, Manna and co-workers have shown that the use of zincblende seeds during the coinjection of seeds and precursor can yield uniform tetrapods with wurtzite arms for a variety of II−VI semiconductors.[36]

In a typical synthesis without seeds, the addition of cadmium and selenium precursors to the reaction flask causes a sudden supersaturation, resulting in a wave of nuclei formation and the consumption of a substantial fraction of the initial reactants. In seed-mediated syntheses, however, the injection of seed nanocrystals provides preformed nucleation sites such that the free cadmium and selenium monomers are not consumed to form nuclei, thus keeping the relative concentrations of these precursors high throughout the initial stages of nanocrystal growth. Previous investigations of the growth kinetics of metal[37] and semiconductor[38] nanocrystals suggest that growth is limited by the rate of reaction between monomeric species and the nanocrystal surface, rather than the mass transport through diffusion processes of those reactive species from the bulk solution to the particle. The reaction rate, in turn, depends on the chemical potential difference between the surface facet and the surrounding reaction mixture. By keeping the monomer concentration high, and thus changing the chemical potential of the reaction mixture at early growth stages, it may be possible to initiate the growth of new particle morphologies by stabilizing or promoting the growth of a different set of surface facets. We propose that such a mechanism may be at work in the following results, in which we detail for the first time the synthesis and characterization of nanocrystalline wz-CdSe hexagonal platelets, cubes, and rods achieved using a seed-mediated synthesis technique. In addition we characterize quantitatively, using semiautomated image analysis tools on transmission electron micrographs, the shape and size distributions of large ensembles of wz-CdSe nanocrystals to unambiguously determine the shape selectivity at each of the synthetic conditions.

EXPERIMENTAL METHODS

Synthesis of wz-CdSe Nanocrystals. Trioctylphosphine oxide (TOPO, 99%), trioctylphosphine (TOP, 90%), cadmium oxide (CdO, >99.99%), and selenium (Se, 99.5%+ 100 mesh) were purchased from Sigma-Aldrich. Hexylphosphonic acid (HPA, lot D039-164) and octadecylphosphonic acid (ODPA, lot n-ODPPA-080002) were purchased from PCI synthesis. All chemicals were used as received without further purification.

Seed Particles. Spherical CdSe seeds were synthesized using a method similar to that of Manna and co-workers.[35] In a typical synthesis, 3 g TOPO, 0.060 g CdO, and 0.280 g ODPA were degassed at 120 °C for approximately 1 h. The solution was heated under nitrogen to 300 °C, at which point 700 μL of TOP was injected. The solution was then heated to 370 °C, and a premade solution of 0.058 g Se dissolved in 1 mL of TOP was injected to initiate seed nucleation and growth. Depending on the desired size of the nanocrystal seeds, growth continued for approximately 10−120 s before the mixture was cooled to room temperature, to produce monodisperse, quasi-spherical nanocrystals with diameters between 2.4 to 3.5 nm. Representative TEM and absorbance spectra of the seeds can be found in the Supporting Information [SI], Figure S1. Optical spectroscopy was used to confirm the seed nanocrystal diameter and extinction coefficient, using established correlations.[39] The seeds were not purified from the reaction mixture prior to use in the reactions described below. In each injection of the Se-TOP complex, approximately 0.08 μmol of CdSe seeds were added corresponding to 89−160 μL of the liquefied CdSe seed solution, depending on the batch of seeds.

Hexagonal Platelets. CdSe hexagonal platelets were synthesized by degassing 3 g TOPO, 0.091 g CdO, 0.290 g ODPA, and 0.080 g HPA at 115 °C for approximately 1 h. This mixture was heated to 300 °C under nitrogen, at which point 1.0 mL TOP was injected. The reaction flask was then further heated to 370 °C at which point a mixture of 0.30 g Se in 2 mL of TOP and CdSe seed solution was injected to induce nanocrystal growth. The reaction proceeded for 8 min and was cooled to room temperature.

Cubes. CdSe cubes were synthesized by degassing 3 g TOPO, 0.086 g CdO, 0.290 g ODPA, and 0.080 g HPA at 115 °C for approximately 1 h. This mixture was heated to 345 °C under nitrogen, at which point 1.0 mL of TOP was injected. The reaction flask was allowed to equilibrate, and a mixture of 0.30 g Se in 2 mL of TOP and CdSe seed solution was injected to induce nanocrystal growth. The reaction proceeded for 8 min and was cooled to room temperature.

Rods. CdSe rods were synthesized by degassing 3 g TOPO, 0.057 g CdO, 0.290 g ODPA, and 0.080 g HPA at 115 °C for approximately 1 h. This mixture was heated to 350 °C under nitrogen, at which point 1.2 mL of TOP was injected. The reaction flask was allowed to equilibrate, and a mixture of 0.295 g Se in 2.05 mL of TOP and CdSe seed solution was injected to induce nanocrystal growth. The reaction proceeded for 8 min and was cooled to room temperature.

Characterization of wz-CdSe Nanocrystals. A 1:1 mixture of *n*-hexanes and methanol was added to each of the cooled reaction mixtures to induce nanocrystal flocculation. Centrifugation (4000 rpm for 5 min) caused the nanocrystals to precipitate, thus allowing unreacted starting materials, reaction byproducts, and excess surfactant to be decanted off. The particles were redispersed into organic solvents for subsequent cleaning or characterization. Transmission electron microscope (TEM) samples were prepared by dropcasting a dilute nanocrystal dispersion in hexanes on a carbon-coated copper TEM grid (200 mesh, Electron Microscopy Sciences). TEM was performed using a Phillips CM100 Electron Microscope operated at 80 kV; high-resolution TEM (HRTEM) was performed using a JEOL 2000FX microscope equipped with a single tilt sample holder and an accelerating voltage of 200 kV. Optical spectra were obtained using an Ocean Optics 4000 USB UV−vis spectrometer.

X-ray diffraction (XRD) was performed experimentally with a Scintag XDS 2000 X-ray diffractometer. Powder diffraction patterns were simulated for wz-CdSe nanocrystals following Bawendi et al.[20,40] and compared to the experimental spectra. The atomic coordinates used to simulate the diffraction patterns were obtained by generating a bulk wz-CdSe crystal in CrystalMaker (CrystalMaker Software Ltd.) and eliminating atoms to form nanocrystals with the experimentally observed sizes, shapes, and bounding facets. The largest crystals (i.e., the hexagonal platelets) that were simulated had sizes of ∼18 nm by ∼20 nm by ∼11 nm and included greater than 1×10^5 atoms. The diffraction simulations used the Debye formula:[41,42]

$$I(q) = \sum_i \sum_j f_i(q) f_j(q) \frac{\sin(q r_{ij})}{q r_{ij}} \quad (1)$$

where $I(q)$ is the intensity from coherent scattering, and the sums are performed over all atoms i and j with r_{ij} being the distance between atoms. Here $q = 4\pi \sin\theta/\lambda$ is the scattering parameter, in which θ and λ are the angle of reflection and the wavelength of the incident X-rays,

dx.doi.org/10.1021/ja402240m | J. Am. Chem. Soc. 2013, 135, 6669−6676

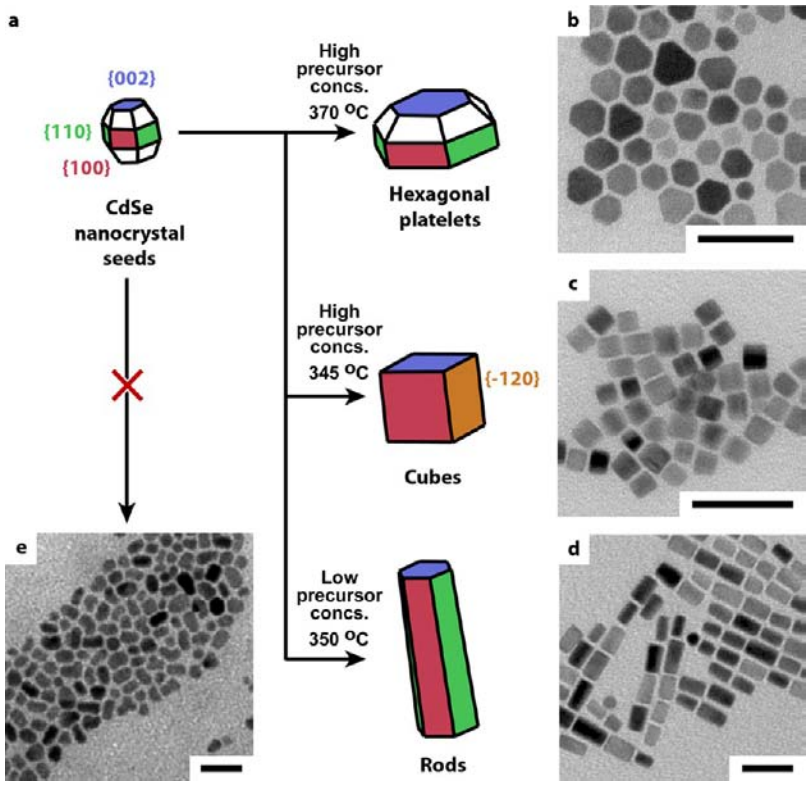

Figure 1. (a) Schematic illustrating the relationship between the geometry and bounding crystal facets (colorized) of the wurtzite CdSe nanocrystal seeds and the nanocrystals produced in the seed-mediated synthesis. Typical TEM images of wz-CdSe nanocrystals with shapes of (b) hexagonal platelets, (c) cubes, and (d) rods. (e) TEM image from a similar synthesis conducted without using the CdSe nanocrystal seeds, resulting in elongated and misshapen particles. The scale bars each correspond to 50 nm.

respectively. The angle-dependent atomic scattering factors f for Cd and Se atoms were approximated by Hartree–Fock wave functions,[43] and the random displacement in the atomic positions due to thermal effects were accounted for with a constant Debye–Waller factor of 0.04 Å^2 for each atom.[44]

Classification of Nanocrystal Size and Shape. Measurements of size- and shape-distributions for each sample were obtained by analyzing multiple TEM images using custom-programmed Matlab (MathWorks, Inc.) code. Image preprocessing was performed in Photoshop CS4 (Adobe Systems, Inc.) or ImageJ (U.S. National Institutes of Health) software to enhance the contrast of the particles against the TEM grid background and to convert the grayscale TEM image into a binary black/white image. The boundary of each particle was defined by 16 line segments to reduce high-frequency noise due to roughness, and then upsampled to 128 segments per particle to increase the number of descriptors. Analysis of a single particle produced various metrics of the particle size, as well as a set of six complex Fourier descriptors that were used to classify nanocrystals as having a specific geometric shape. A quantitative analysis of the size- and shape-distributions allowed for a determination of the selectivity of the specified synthetic conditions toward a certain shape. A more extensive description of this technique for the large-scale, semi-automated characterization of nanoparticle shape has been reported elsewhere.[45]

■ RESULTS AND DISCUSSION

The combination of control over both the reaction chemistry and the nucleation stage—through the appropriate choice and concentration of phosphonic acids and preformed CdSe nanocrystal seeds—allows tailoring of the seed-mediated growth of larger wurtzite CdSe nanocrystals to produce a variety of well-defined shapes. The schematic in Figure 1a illustrates how reaction conditions may be tuned to produce nanosized hexagonal platelets, cubes, and nanorods (b–d of Figure 1, respectively) by controlling the addition of cadmium and selenium monomer species onto seed nanocrystals. In contrast, when preformed CdSe nanocrystal seeds are omitted from the reaction, the resulting particles are polydisperse in both shape and size, consisting of a mix of bent and malformed low-aspect ratio rods, spheroidal particles, and a small number of branched particles (Figure 1e).

It is clear that the Wulff construction for bulk CdSe, in which the morphology of a growing crystal can be determined by the surface energies of the growing facets when in thermodynamic equilibrium, cannot fully explain the variety of shapes observed here, as it does not account for nonequilibrium kinetic effects or the energetic and steric contributions of the phosphonic acid capping ligands to the growth. Many factors in the synthesis can contribute to the final shape, such as the seeds that control the nucleation, growth temperature, growth time, monomer concentrations, and binding characteristics of the surfactants that are used. In previous work, shape was controlled by altering the relative concentration of monomers in the reaction mixture, yielding shapes such as rods, wires, and tetrapods.[29] At low concentrations of monomer in solution, spherical nanocrystals typically form. As the concentration of monomer increases, metastable structures can form, where the monomers add to specific facets causing one dimensional (1D) growth and result in rodlike structures. Using a seed-mediated growth procedure, we also have control over the number of nuclei available to form nanocrystals, simply because the activation energy barrier for addition of monomers to preformed seeds is much lower compared to the energetic barrier for precursors to form separate nuclei.[35]

dx.doi.org/10.1021/ja402240m | J. Am. Chem. Soc. 2013, 135, 6669–6676

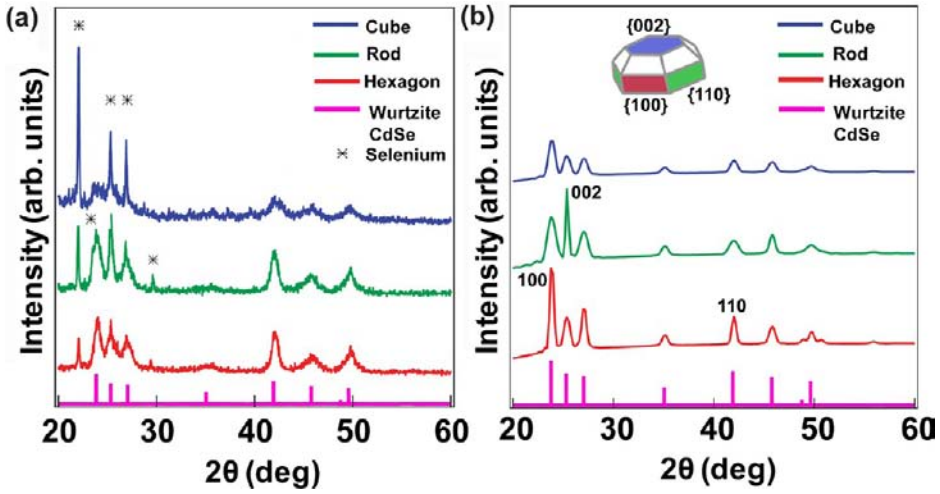

Figure 2. XRD spectra of wurtzite CdSe nanocrystals with shapes of cubes, rods, and hexagonal platelets. (a) Experimental powder spectra of the as-synthesized nanocrystals and (b) simulated spectra for single-crystalline particles of the same average size. Theoretical peaks for wz-CdSe are shown as magenta lines below the spectra,[46] and peaks attributed to unreacted Se are marked with an asterisk (*).

Hexagonal Platelets. Hexagonal platelets of wz-CdSe were synthesized selectively at the highest growth temperatures (370 °C, when the Se/TOP/CdSe seed mixture was injected into the reactor) and highest Cd concentrations. The nanocrystals grow with lower index facets to minimize overall energy, thus leading to highly faceted particles[28] so that a hexagonal platelet may be a way for the crystal to maintain stability under high-temperature conditions. The composition and crystal structure of the hexagonal platelets was confirmed by X-ray diffraction. A typical XRD spectrum of the hexagonal platelets is shown in Figure 2a, with a series of broad peaks corresponding to nanosized CdSe with a wurtzite crystal structure.[46] There are an additional five sharp peaks (marked with an asterisk at 2θ positions of 22.04, 23.58, 25.5, 26.86, 29.02) that can be attributed to submicrometer-sized particles of monoclinic Se,[47,48] likely due to small amounts of unreacted Se that were not fully removed from the sample during postsynthesis purification. A diffraction pattern simulated for a hexagonal platelet with the specified wurtzite CdSe crystal structure, bounding facets, and average particle size is shown in Figure 2b. The simulated pattern shows that the sharpest and most intense peaks are associated with the (100) and (110) planes of the wz-CdSe hexagonal platelets, which correspond well to the powder diffraction spectra as a result of the radial dimension of the platelet being nearly twice that of the thickness.

A low-magnification TEM image of the hexagonal platelets is shown in Figure 3a, demonstrating the monodisperse size and shapes of the platelets across an extended area of the grid. In this image, platelets can be seen in which the largest face of the platelet lies flat on the carbon-coated TEM grid, as well as platelets that form extended chains with a face-to-face arrangement (i.e., the largest faces oriented perpendicular to the substrate). The face-to-face ordering is characteristic of platelets at moderate surface coverages on substrates; at higher concentrations, the chains themselves also begin to assemble into hexagonal arrays, forming structures analogous to a columnar liquid crystal phase.[49,50] High-resolution TEM images of individual platelets are shown in b and c of Figure 3, in which the largest (002) face is perpendicular and parallel to the beam direction, respectively. The basis for an atomistic model of the platelet is shown in the insets. The calculated fast Fourier transform (FFT) spectra of the HRTEM images (d and e of

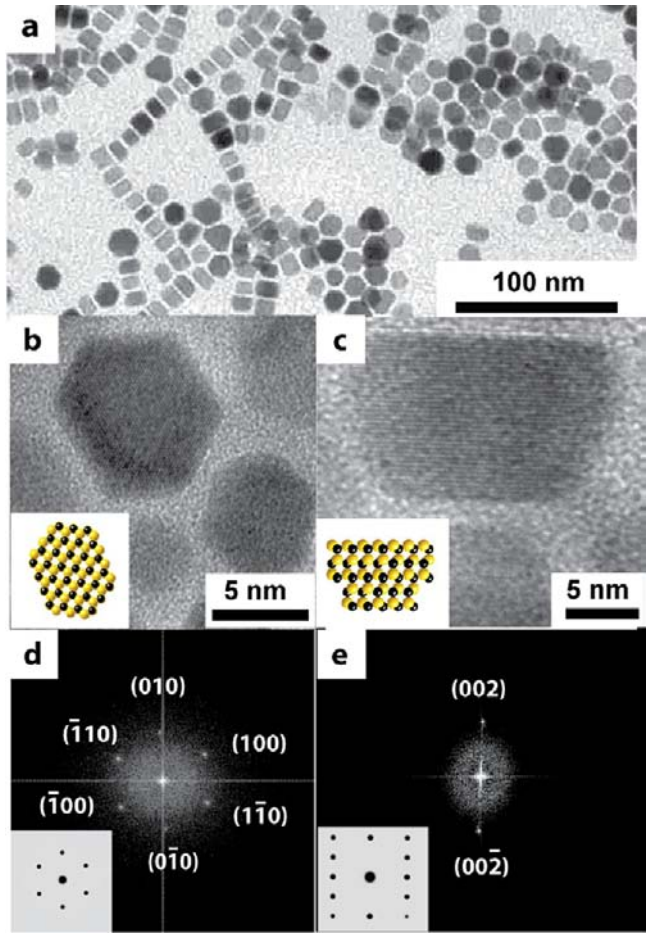

Figure 3. (a) TEM image of hexagonal platelet-shaped wurtzite CdSe nanocrystals containing areas in which the faces are perpendicular or parallel to the substrate. HRTEM images of wz-CdSe platelets with the (002) face oriented (b) parallel and (c) perpendicular to the substrate, with the insets showing atomistic models of the crystal structure in each case. (d, e) FFT spectra of the atomic arrangement from the HRTEM images (b, c respectively) match closely with the diffraction patterns calculated from the atomistic models (insets).

dx.doi.org/10.1021/ja402240m | J. Am. Chem. Soc. 2013, 135, 6669−6676

Figure 3) and the simulated electron diffraction patterns (insets) show excellent agreement. The peak positions and atomic lattice spacings quantified in the FFT spectra confirm the wurtzite crystal structure of the wz-CdSe platelets, and were used to determine the bounding facets of the nanoparticles. In Figure 3b the platelet is viewed along the ⟨002⟩ zone axes. The geometry of the side facets, arranged at approximately 120° angles to one another, indicates they are made up from the {100} and {010} planes as summarized in Figure 1a. The side facets can be directly observed with HRTEM in Figure 3c, and as expected, these side bounding planes in a wurtzite crystal structure intersect the top (002) and bottom (00−2) faces at an ∼90° angle.[51]

Recently, zincblende CdSe platelets were synthesized using a seed-mediated method, with the proposed mechanism being that precursors add to the seeds and that the seed diameter sets the thickness for the entire platelet.[52] These platelets did not have a defined crystal facet structure and were much larger. We propose that a similar mechanism takes place in the synthesis of our wurtzite CdSe hexagonal platelets, where the injected seeds dictate the final platelet thickness and growth occurs radially in the [100] and [010] crystal directions. The (002) face may be more Cd-rich and therefore more highly passivated by the alkylphosphonic acid ligands, and thus not as favorable for precursor addition. In addition, it is observed that the (002) top face is smaller than the (00−2) bottom face, because the platelets appear to assume a trapezoidal shape as they stack on their sides into chains.

Cubes. Monodisperse wurtzite CdSe nanocubes (Figure 1c) were synthesized with reaction conditions (e.g., reactant and ligand concentrations) similar to that of the platelet synthesis, but at lower growth temperatures (345 °C). Diffraction spectra and simulated patterns (blue curves in Figure 2) for the wz-CdSe nanocubes match closely with a most intense signal arising due to diffraction from the (100) plane, but overall have broader and less intense peaks due to the relatively smaller size of this morphology. Characterization of the nanocubes using HRTEM in Figure 4a shows that the particles do not contain significant numbers of lattice defects. The FFT of the HRTEM image (Figure 4c) reveals a pattern corresponding to the diffraction of a hexagonal crystal structure taken along the [−120] direction; assignment of the arrangement and position of the diffraction spots in the spectra allow us to identify bounding facets on the cube as the {002}, {100}, and {−120} facets. It is notable that this diffraction pattern is characteristic of hexagonal crystal systems and is not found in crystal systems with cubic symmetry, offering further confirmation that the nanocubes do have a wurtzite crystal structure. Further, while we have termed these objects "cubes", the corners appear to show some rounding, suggesting that there may be some truncation of the edges and corners that cannot be fully resolved.

Although the appearance of the {−120} facets is somewhat unexpected for nanoscale particles with a wurtzite crystal structure, examination of the underlying geometry of the wurtzite system confirms that these planes are oriented orthogonally to each other and can occur as the bounding facets in the physical particles. The simulated electron diffraction pattern from an atomistic model of a wurtzite CdSe nanocube built using these bounding facets (b and d of Figure 4) shows good qualitative agreement with the HRTEM images and the experimentally determined diffraction pattern. Intriguingly, the experimentally measured lattice plane *d*-spacings from the HRTEM images are all approximately 0.1−0.2 Å *less* than those measured for bulk wurtzite CdSe; for example, we measure *d*-spacings of 3.52Å for the (100) plane compared with 3.72 Å in the bulk, 3.29 Å for the (002) plane compared with 3.51 Å in the bulk, and 2.39 Å for the (102) plane compared with 2.55 Å in the bulk. A similarly large reduction in the lattice spacing was also recently observed by Hyeon and co-workers in templated CdSe platelets[53] and may be caused during growth by compressive stresses within the particle that can reduce the *d*-spacing and influence the final particle morphology.[54,55] These compressive stresses, which are caused by ligand binding at the surface, may also influence the relative surface energies of various facets in the particle during the growth process—in addition to those normal steric and energetic effects due to the presence of the capping ligand—allowing facets such as the {−120} that are less energetically favorable in the bulk to emerge at the nanoscale.

Rods and Bullets. Seed-mediated syntheses at low reaction temperatures (350 °C), and lower concentrations of the cadmium precursor drive the wz-CdSe particle morphology away from cubes and toward the more commonly observed nanorod (Figure 1d) or tapered nanorod ("bullet") shapes. High-resolution TEM images of such structures are shown in Figure 5 and in the SI (Figure S2). Under these synthetic conditions, preferential growth occurs longitudinally in the

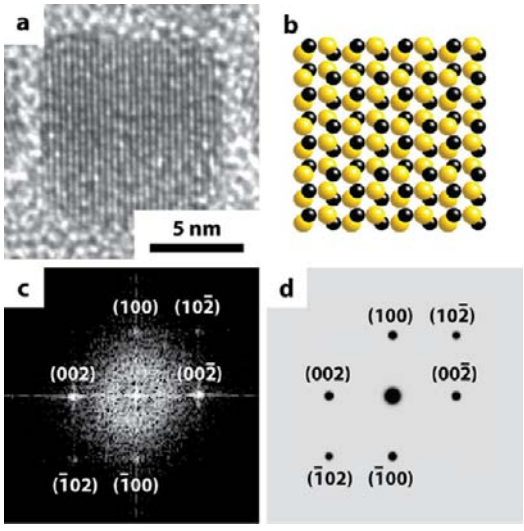

Figure 4. Characterization of wurtzite CdSe nanocubes. (a) HRTEM image and (c) FFT spectrum compared to (b) an atomistic model and (d) the corresponding calculated diffraction pattern.

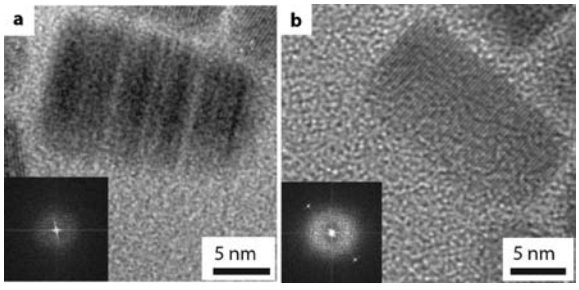

Figure 5. High-resolution TEM images of a wurtzite CdSe (a) bullet and (b) nanorod. Calculated FFT diffraction patterns of the bullet and nanorod are shown in the insets.

dx.doi.org/10.1021/ja402240m | J. Am. Chem. Soc. 2013, 135, 6669−6676

⟨002⟩ crystal direction, and the side facets are made up of the {100} and {010} planes. Powder diffraction spectra and simulated patterns (green curves in Figure 2) for the wz-CdSe nanorods both exhibit an intense, sharp signal arising due to diffraction from the (002) plane, indicating significant elongation in that direction. The (100) peaks in the rod spectra are also significantly broadened compared to the platelet spectra, indicating smaller dimensions in the radial direction.

Prior investigation of elongated morphologies by Scholes and co-workers[56] made use of both carboxylic and phosphonic acids as growth-directing agents, and they proposed that the carboxylic acid group binds to the faster growing {001} facets and is more labile than the phosphonic acids.[28] Faster growth on the (00−1) facet compared to that on the (001) facet resulted in the tapered shapes that were observed. We propose that the hexylphosphonic acid in our synthesis fills a role similar to that of the carboxylic acid in the synthesis by Scholes and co-workers.[56] Compared with the longer octadecylphosphonic acid, which makes up the majority of the phosphonic acids present in our synthesis, the HPA is expected to have a higher adsorption/desorption rate which induces growth faster at the sites to which it binds, yielding rods because precursors preferentially add to the (002) and the (00−2) facets. Bulletlike structures are formed when precursors can add fastest to the (00−2) facet, whereas the (002) facet remains square and rodlike. The (002) and (00−2) crystal facets grow at different rates because the Cd-rich (002) facet is more highly passivated by the phosphonic acids and the less passivated Se-rich (00−2) facet can allow for more precursor addition.[57,58] While the seed particles cannot be observed directly in the HRTEM images because of identical lattice structures and the occurrence of epitaxial growth, CdS/CdSe rods synthesized in a similar method have shown that the seed position is located at 1/3 to 1/4 of the length of the final rod, suggesting anisotropic precursor addition to the (002) and (00−2) facets.[35] Since the surface energy is significantly higher on the (00−2) in wurtzite CdSe,[53] we can expect precursor to typically add to that face. We also suggest that the growth of surface oxides on the CdSe seeds, or other surface effects that gradually appear, may influence the balance between nanorod and bullet growth. The first exciton peak in the UV−vis spectra of the seed nanocrystals slightly red-shifts over the course of a few months, suggesting some particle ripening, oxidation, or other effects may be occurring. Under identical reaction conditions, these "aged" seeds tend to create more bulleted shapes than their freshly synthesized counterparts.

Quantitative Analysis of Nanocrystal Shape and Size. The shapes of the wz-CdSe nanocrystals were classified quantitatively and in a high-throughput manner using an automated method based on complex Fourier descriptors. This morphometric approach for classifying nanocrystal shape has been shown to eliminate the ambiguity and subjectiveness of manual classification and is capable of providing quantitative information.[45] Hundreds or thousands of nanocrystals can be rapidly analyzed from individual or sequences of TEM images, thereby enabling the measured distributions of size and shape to be statistically representative of the entire nanocrystal system. In this shape characterization method, the complex Fourier transform of the particle boundary was taken to obtain magnitudes of the low-order Fourier descriptors, which can be correlated to physical characteristics such as squareness, triangularity, or elongation. The particles were sorted on the basis of their Fourier descriptor magnitudes into shape categories (e.g., hexagon, pentagon, rod, square, triangle, circle, and ellipse), and a colormap of the TEM image was generated with the particles classified by their shape. Information about particle perimeter, area, aspect ratio, and size was also calculated from the TEM image.

Figure 6 shows an original TEM image and the corresponding map of the nanocrystals colorized by shape. A

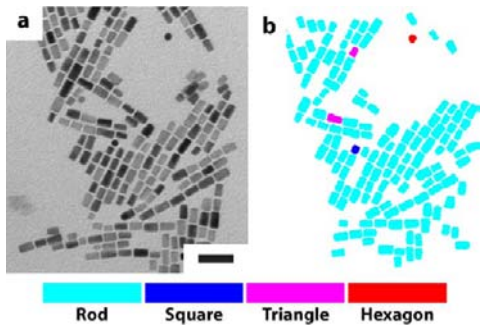

Figure 6. Characterization of nanocrystal shape using (a) a TEM image of wz-CdSe nanorods from a seed-mediated synthesis and (b) the corresponding colormap of the classified nanocrystal shapes. The scalebar in (a) applies to both images and represents 50 nm. The color scale at the bottom of the figure indicates the shape classifications considered by the Fourier descriptor analysis of the individual particles.

total of 142 individual nanocrystals were analyzed in the image, yielding 97% rods, 1% squares, 1% triangles (tapered rods in this case), and 1% hexagons. An aspect ratio of 1.3 was chosen to distinguish elongated from compact forms of each shape, i.e. squares from rods and circles from ellipses. The analysis of the image also yielded an average particle diameter of 13 ± 2 nm, an average length 22 ± 4 nm, and aspect ratio of 1.7 ± 0.2. Table 1 contains quantitative results on the yield of the

Table 1. Shape Yield, Diameter, and Aspect Ratio for wz-CdSe Nanocrystals Synthesized by Seedless- and Seed-Mediated Mechanisms, As Quantified by High-Throughput Image Analysis of Transmission Electron Micrographs

primary shape	yield of primary shape (%)	size ($D \pm \sigma$) (nm)	aspect ratio $\pm \sigma$
seedless synthesis	not applicable; irregular	8 ± 2	1.6 ± 0.3
hexagonal platelets	89	16 ± 3	1.1 ± 0.1
cubes	82	12 ± 1	1.1 ± 0.1
rods	97	13 ± 2	1.7 ± 0.2
bullets	~31[a]	13 ± 3	1.8 ± 0.4

[a]Automated classification of nanocrystal shape was prevented by the overlap of neighboring nanocrystals during imaging; yield was determined manually.

predominant shape, average diameter, and average aspect ratio of the CdSe nanocrystals for each of the seed-mediated shape-directed syntheses introduced above. The complete distributions of nanocrystal shape and size for each synthesis can be found in the SI (Figure S3).

Although assignment of nanocrystal shape by complex Fourier descriptors is robust when using low-resolution TEM images and relatively independent of surface texture or noise in the nanocrystal boundary (either real or introduced through the imaging technique), there are some challenges with this

approach.[45] Nanocrystals that physically overlapped or that had poor contrast with the background were impossible to isolate and thus were excluded from the analysis so as to not influence the shape assignments and size distributions (indicated by voids in the colormap of shapes). The success of automated shape classification is therefore dependent on the quality of the images acquired by the nanoscale characterization technique and image postprocessing with filter and watershed functions. In addition, any manual or automated shape classification approach based on TEM analysis considers 2D projections of 3D objects and does not account for the various orientations that can be adopted by anisotropic shapes (e.g., the rods and hexagonal platelets) on the substrate. For example, a nanocrystal rod projected in two dimensions might either appear as an elongated rectangular structure when oriented parallel to the substrate or as a hexagonal or round particle when oriented perpendicular to the substrate.

CONCLUSIONS

A seed-mediated growth mechanism was used to synthesize wurtzite CdSe nanocrystals with diverse shapes. Seed-mediated growth provided control over the nucleation step, allowing a high monomer concentration to be maintained throughout the nucleation process and enabling preferential precursor addition to facets of wz-CdSe that are not normally favored or available for growth. Hexagonal platelets, cubes, and rods of wz-CdSe nanocrystals were produced by controlling the synthetic conditions, including the seed and precursor concentrations, reaction temperature, seed size, and growth time. Syntheses performed at high reaction temperatures by the rapid injection of seeds and precursors led to more highly faceted hexagonal particles, and at lower reaction temperatures the use of higher precursor concentrations favored the synthesis of cubes over nanorods. Using small wz-CdSe seeds, the hexagonal platelets were formed by growth radially from the (002) face, which differs from the growth mechanism for nanorods in which the precursor added axially to the (002) face. Nanocubes were synthesized that exhibited {100}, {002}, and {−120} bounding facets, illustrating that control over surface chemistry and the nucleation stage can give rise to nanocrystals with faceting that is atypical and does not correspond to the lowest surface energies in the bulk system. The shape and size of the synthesized wz-CdSe nanocrystals were characterized quantitatively, and the seed-mediated growth conditions presented here resulted in >80% selectivity for the majority shape. In addition, the seed-mediated synthesis of wz-CdSe nanocrystals with controlled shapes described here is highly robust and reproducible, having been achieved in multiple reaction batches performed over the course of a long time frame (>1 year).

The discovery of synthetic methods for generating wz-CdSe nanocrystals with these shapes, that were heretofore unattainable, is likely to result in materials with unique optical, electronic, and catalytic properties dependent on the specific crystal form (i.e., crystal structure, particle shape, and particle size). The platelet and cube morphologies are also attractive for the self assembly of nanocrystal arrays or superlattices with high packing densities that may prove useful for the fabrication of optoelectronic devices in thin films or in the bulk. Due to previously observed similarities in synthetic techniques and shape control between CdSe and the other cadmium chalcogenides, there is the possibility that the methods presented here could also give rise to similar shapes for CdS and CdTe, and heterostructured materials.

ASSOCIATED CONTENT

Supporting Information

Synthetic details and characterization (UV−vis and TEM) of the CdSe seed nanocrystals, TEM characterization of bullet-shaped wz-CdSe nanocrystals, and the distribution of aspect ratios for wz-CdSe nanocrystals of each shape. This material is available free of charge via the Internet at http://pubs.acs.org.

AUTHOR INFORMATION

Corresponding Author

mark.stoykovich@colorado.edu

Present Address

[†]Applied Chemicals and Materials Division, National Institute of Standards and Technology, Boulder, CO 80305, United States.

Notes

The authors declare no competing financial interest.

ACKNOWLEDGMENTS

We thank Dr. Roy Geiss at the University of Colorado's Nanomaterials Characterization Facility (NCF) for assistance with the HRTEM characterization and Ian Campbell for assistance with the XRD measurements. K.P.R. thanks ConocoPhillips for financial support.

REFERENCES

(1) Cozzoli, P. D.; Pellegrino, T.; Manna, L. *Chem. Soc. Rev.* **2006**, *35*, 1195−1208.
(2) Costi, R.; Saunders, A. E.; Banin, U. *Angew. Chem., Int. Ed.* **2010**, *49*, 4878−4897.
(3) Norris, D. J.; Efros, A. L.; Erwin, S. C. *Science* **2008**, *319*, 1776−1779.
(4) Xie, R. G.; Peng, X. G. *J. Am. Chem. Soc.* **2009**, *131*, 10645−10651.
(5) Manna, L.; Scher, E. C.; Alivisatos, A. P. *J. Am. Chem. Soc.* **2000**, *122*, 12700−12706.
(6) Peng, X. G.; Manna, L.; Yang, W. D.; Wickham, J.; Scher, E.; Kadavanich, A.; Alivisatos, A. P. *Nature* **2000**, *404*, 59−61.
(7) Manna, L.; Scher, E. C.; Alivisatos, A. P. *J. Cluster Sci.* **2002**, *13* (4), 521−532.
(8) Hutter, E.; Fendler, J. H. *Adv. Mater.* **2004**, *16*, 1685−1706.
(9) Tian, N.; Zhou, Z. Y.; Sun, S. G.; Ding, Y.; Wang, Z. L. *Science* **2007**, *316*, 732−735.
(10) Narayanan, R.; El-Sayed, M. A. *J. Phys. Chem. B* **2005**, *109*, 12663−12676.
(11) Joo, S. H.; Park, J. Y.; Tsung, C. K.; Yamada, Y.; Yang, P. D.; Somorjai, G. A. *Nat. Mater.* **2009**, *8*, 126−131.
(12) Hu, J. T.; Li, L. S.; Yang, W. D.; Manna, L.; Wang, L. W.; Alivisatos, A. P. *Science* **2001**, *292*, 2060−2063.
(13) Kazes, M.; Lewis, D. Y.; Ebenstein, Y.; Mokari, T.; Banin, U. *Adv. Mater.* **2002**, *14*, 317−321.
(14) Buhro, W. E.; Colvin, V. L. *Nat. Mater.* **2003**, *2*, 138−139.
(15) Huynh, W. U.; Dittmer, J. J.; Alivisatos, A. P. *Science* **2002**, *295*, 2425−2427.
(16) Gur, I.; Fromer, N. A.; Geier, M. L.; Alivisatos, A. P. *Science* **2005**, *310*, 462−465.
(17) Anikeeva, P. O.; Halpert, J. E.; Bawendi, M. G.; Bulovic, V. *Nano Lett.* **2009**, *9*, 2532−2536.
(18) Murray, C. B.; Kagan, C. R.; Bawendi, M. G. *Annu. Rev. Mater. Sci.* **2000**, *30*, 545−610.
(19) Baranov, D.; Fiore, A.; van Huis, M.; Giannini, C.; Falqui, A.; Lafont, U.; Zandbergen, H.; Zanella, M.; Cingolani, R.; Manna, L. *Nano Lett.* **2010**, *10* (2), 743−749.
(20) Murray, C. B.; Norris, D. J.; Bawendi, M. G. *J. Am. Chem. Soc.* **1993**, *115*, 8706−8715.

(21) Yin, Y.; Alivisatos, A. P. *Nature* **2005**, *437*, 664−670.
(22) Manna, L.; Wang, L. W.; Cingolani, R.; Alivisatos, A. P. *J. Phys. Chem. B* **2005**, *109*, 6183−6192.
(23) Rempel, J. Y.; Trout, B. L.; Bawendi, M. G.; Jensen, K. F. *J. Phys. Chem. B* **2006**, *110*, 18007−18016.
(24) Shieh, F.; Saunders, A. E.; Korgel, B. A. *J. Phys. Chem. B* **2005**, *109*, 8538−8542.
(25) Qian, C.; Kim, F.; Ma, L.; Tsui, F.; Yang, P. D.; Liu, J. *J. Am. Chem. Soc.* **2004**, *126*, 1195−1198.
(26) Yang, Y. A.; Wu, H. M.; Williams, K. R.; Cao, Y. C. *Angew. Chem., Int. Ed.* **2005**, *44*, 6712−6715.
(27) Ithurria, S.; Dubertret, B. *J. Am. Chem. Soc.* **2008**, *130*, 16504−16505.
(28) Liu, L. P.; Zhuang, Z. B.; Xie, T.; Wang, Y. G.; Li, J.; Peng, Q.; Li, Y. D. *J. Am. Chem. Soc.* **2009**, *131*, 16423−16429.
(29) Peng, X. G. *Adv. Mater.* **2003**, *15*, 459−463.
(30) Rao, C. N. R.; Govindaraj, A.; Deepak, F. L.; Gunari, N. A.; Nath, M. *Appl. Phys. Lett.* **2001**, *78*, 1853−1855.
(31) Talapin, D. V.; Nelson, J. H.; Shevchenko, E. V.; Aloni, S.; Sadtler, B.; Alivisatos, A. P. *Nano Lett.* **2007**, *7*, 2951−2959.
(32) Kanaras, A. G.; Sonnichsen, C.; Liu, H.; Alivisatos, A. P. *Nano Lett.* **2005**, *5*, 2164−2167.
(33) Deka, S.; Miszta, K.; Dorfs, D.; Genovese, A.; Bertoni, G.; Manna, L. *Nano Lett.* **2010**, *10*, 3770−3776.
(34) Miszta, K.; de Graaf, J.; Bertoni, G.; Dorfs, D.; Brescia, R.; Marras, S.; Ceseracciu, L.; Cingolani, R.; van Roij, R.; Dijkstra, M.; Manna, L. *Nat. Mater.* **2011**, *10*, 872−876.
(35) Carbone, L.; Nobile, C.; De Giorgi, M.; Sala, F. D.; Morello, G.; Pompa, P.; Hytch, M.; Snoeck, E.; Fiore, A.; Franchini, I. R.; Nadasan, M.; Silvestre, A. F.; Chiodo, L.; Kudera, S.; Cingolani, R.; Krahne, R.; Manna, L. *Nano Lett.* **2007**, *7*, 2942−2950.
(36) Fiore, A.; Mastria, R.; Lupo, M. G.; Lanzani, G.; Giannini, C.; Carlino, E.; Morello, G.; De Giorgi, M.; Li, Y.; Cingolani, R.; Manna, L. *J. Am. Chem. Soc.* **2009**, *131*, 2274−2282.
(37) Saunders, A. E.; Sigman, M. B.; Korgel, B. A. *J. Phys. Chem. B* **2004**, *108*, 193−199.
(38) Bullen, C. R.; Mulvaney, P. *Nano Lett.* **2004**, *4*, 2303−2307.
(39) Yu, W. W.; Qu, L. H.; Guo, W. Z.; Peng, X. G. *Chem. Mater.* **2003**, *15*, 2854−2860.
(40) Bawendi, M. G.; Kortan, A. R.; Steigerwald, M. L.; Brus, L. E. *J. Chem. Phys.* **1989**, *91* (11), 7282−7290.
(41) Guinier, A. *X-Ray Diffraction*; Freeman: San Francisco, CA, 1963.
(42) Hall, B. D.; Monot, R. *Computers in Physics* **1991**, *5*, 414−417.
(43) Cromer, D. T.; Mann, J. B. *Acta Crystallogr., Sect. A* **1968**, *24*, 321−324.
(44) Vetelino, J. F.; Guar, S. P.; Mitra, S. S. *Phys. Rev. B* **1972**, *5*, 2360−2366.
(45) Rice, K. P.; Saunders, A. E.; Stoykovich, M. P. *Cryst. Growth Des.* **2012**, *12* (2), 825−831.
(46) JCPDS International Centre for Diffraction Data, 2002, card 65-3415.
(47) JCPDS International Centre for Diffraction Data (ICDD); 2002, cards 76-1865 and 24-1202.
(48) Ding, Y.; Li, Q.; Jia, Y.; Chen, L.; Xing, J.; Qian, Y. *J. Cryst. Growth* **2002**, *241*, 489−497.
(49) Puntes, V. F.; Zanchet, D.; Erdonmez, C. K.; Alivisatos, A. P. *J. Am. Chem. Soc.* **2002**, *124*, 12874−12880.
(50) Saunders, A. E.; Ghezelbash, A.; Smilgies, D. M.; Sigman, M. B.; Korgel, B. A. *Nano Lett.* **2006**, *6*, 2959−2963.
(51) Hammond, C. *The Basics of Crystallography and Diffraction*; Oxford Science Publications: Oxford, England, 1997.
(52) Ithurria, S.; Bousquet, G.; Dubertret, B. *J. Am. Chem. Soc.* **2011**, *133*, 3070−3077.
(53) Son, J. S.; Wen, X. D.; Joo, J.; Chae, J.; Baek, S. I.; Park, K.; Kim, J. H.; An, K.; Yu, J. H.; Kwon, S. G.; Choi, S. H.; Wang, Z. W.; Kim, Y. W.; Kuk, Y.; Hoffmann, R.; Hyeon, T. *Angew. Chem., Int. Ed.* **2009**, *48*, 6861−6864.
(54) Meulenberg, R. W.; Jennings, T.; Strouse, G. F. *Phys. Rev. B* **2004**, *70*, 235311.
(55) Zhang, J. Y.; Wang, X. Y.; Xiao, M.; Qu, L.; Peng, X. *Appl. Phys. Lett.* **2002**, *81*, 2076−2078.
(56) Nair, P. S.; Fritz, K. P.; Scholes, G. D. *Small* **2007**, *3*, 481−487.
(57) Scher, E. C.; Manna, L.; Alivisatos, A. P. *Philos. Trans. R. Soc. A* **2003**, *361*, 241−255.
(58) Rosenthal, S. J.; McBride, J.; Pennycook, S. J.; Feldman, L. C. *Surf. Sci. Rep.* **2007**, *62*, 111−157.